CONFERENCE PRE-PRINT

OBSERVATION OF PLASMA PERFORMANCE IMPROVEMENT BY EDGE ECRH POWER DEPOSITION ON EXPERIMENTAL ADVANCED SUPERCONDUCTING TOKAMAK

Y. L. Li*, G. S. Xu*, G. S. Li, Y. Q. Chu, H. L. Zhao, N. Yan, Y. F. Wang, X. L. Zou[‡], Q. Zang, T. Zhang, W. M. Zhang, Z. Zhou, K. X. Ye, W. Y. Xu, D. A. Lu, S. Y. Fu, C. Z. Lin, L. Q. Xu, R. Chen, X. L. Li, R. Ding, L. Wang, Q. Q. Yang, S. X. Wang, Y. M. Duan, L. Zhang, H. Q. Liu, X. Z. Gong, J. S. Hu, Y. T. Song, B. N. Wan, and the EAST team

Institute of Plasma Physics, Chinese Academy of Sciences, Hefei 230031, China

[‡]CEA, IRFM, F-13108 Saint-Paul-lez-Durance, France

*Email: ylli@ipp.ac.cn and gsxu@ipp.ac.cn

Abstract

Edge electron cyclotron resonance heating (ECRH) has been observed to enhance plasma performance on the Experimental Advanced Superconducting Tokamak (EAST). By adjusting the ECRH mirror, the power deposition was shifted from the core to the edge region during H-mode operation. This edge ECRH deposition resulted in a reduction of plasma density and tungsten impurity levels, while simultaneously steepening the electron and ion temperature profiles, thereby improving overall confinement. Correspondingly, the core safety factor increased, leading to the formation of a negative magnetic shear in the core, which is attributed to suppressing the ion temperature gradient (ITG) turbulence, as confirmed by poloidal correlation reflectometry (PCR) diagnostics. Theoretical simulations indicate the coexistence of density gradient-driven trapped electron mode (TEM) turbulence in the core ($\rho_t < 0.45$) and ITG turbulence at the edge ($\rho_t > 0.45$). Suppression of these turbulences contribute to the enhancement of plasma confinement, which results in a significant reduction of the inward convective velocity of tungsten.

1. INTRODUCTION

A key challenge for future fusion reactors, lies in operating a clean plasma in high performance and steady state. The International Thermonuclear Experimental Reactor (ITER), representing a pivotal step in this endeavor, has decided to change the first wall material from beryllium to tungsten (W) and use primarily ECRH [1]. For ignition to be achieved, heavy impurities, such as tungsten, is required to pump out from the confined plasma to avoid high power losses through impurity radiation. Unlike other auxiliary heating systems, such as lower hybrid current drive (LHCD), neutral beam injection (NBI), and ion cyclotron resonance frequency (ICRF) heating, ECRH can efficiently deposit energy into the plasma core while hardly interact with the boundary plasma, thus reducing the impact on plasma-wall interactions. Besides, the tungsten central accumulation can be controlled by core ECRH deposition [2]. The underlying physics is attributed to the rise of impurity outward convection [3,4] and the effect of both the ionization balance and turbulence transport [5]. However, as the toroidal magnetic field strength increases in next-generation fusion devices, achieving core ECRH requires higher gyrotron frequencies, leading to substantial increases in both the complexity and cost of the heating systems. This inherent scaling limitation prompts the exploration of alternative ECRH strategies.

Previous experiments on several tokamaks, including AUG [6,7], TCV [8], and DIII-D [9], have investigated edge ECRH power deposition as a potentially cost-effective alternative. However, these efforts have often led to a deterioration in plasma confinement as ECRH power was shifted to the edge. This presentation reports on a promising edge ECRH power deposition experiment conducted on EAST[10], where an improvement in plasma confinement and a reduction in tungsten central accumulation was achieved. This paper is organized as follows. Section 2 introduces the experimental setup of the edge ECRH deposition experiment in EAST. Section 3 shows the simulations carried out by ONETWO, TGLF[11] and NEO[12] to analysis the thermal diffusivities, turbulence characteristics and tungsten neo-classical transport, respectively. Finally, a discussion and conclusion is given in Section 4.

2. EDGE ECRH DEPOSITION EXPERIMENT

2.1. Experimental setup

In the EAST tokamak, we have conducted an ECRH edge power deposition experiment as seen on Fig. 1. The plasma was configured in an upper single null geometry with plasma current I_p of 500kA. The background

auxiliary heating powers consisted of LHCD power $P_{LHW}=1.5$ MW and NBI power $P_{NB}=2.6$ MW, as shown in Fig. 1(f-1, 2, 3). The ECRH deposition location was varied by adjusting both the ECRH mirror angle and the toroidal magnetic coil current I_t . Specifically, the toroidal/poloidal ECRH mirror angles were set to $20^{\circ}/103^{\circ}$ for core deposition and $20^{\circ}/85^{\circ}$ for edge deposition. The toroidal magnetic coil current I_t was varied among three values, i.e., -11kA, -10.5kA and -10kA, which corresponds to toroidal magnetic fields of 2.4 T, 2.3 T and 2.2T, respectively. Consequently, the edge safety factor q_{95} shifted from 5.2 to 4.7. These adjustments shifted the ECRH deposition position from $\rho_{EC}=0$ to $\rho_{EC}=0.8$. The ECRH power was modulated from 0.3MW to 0.6MW at frequencies of 5 Hz and 10 Hz and injected into the H-mode plasma at time=3.1s.

Following the ECRH heating, the internal induction l_i , as shown in Fig. 1(c-1, 2, 3), initially decreased and then recovered. For the cases with more outward deposition of ECRH, the reduction of l_i is much larger, implying a flatten of the plasma current profile. Interestingly, both the plasma density (Fig. 1(a-1, 2, 3)) and the tungsten impurity (Fig. 1(e-1, 2, 3)) were reduced to a lower level under off-axis ECRH deposition, suggesting that this approach effectively pumps out the particles and impurities from the core plasma. At these reduced tungsten impurity levels, the plasma stored energy (Fig. 1(b-1, 2, 3)) was significantly enhanced. Note that the loop voltage (Fig. 1(d-1, 2, 3)) was not reduced after the ECRH injection.

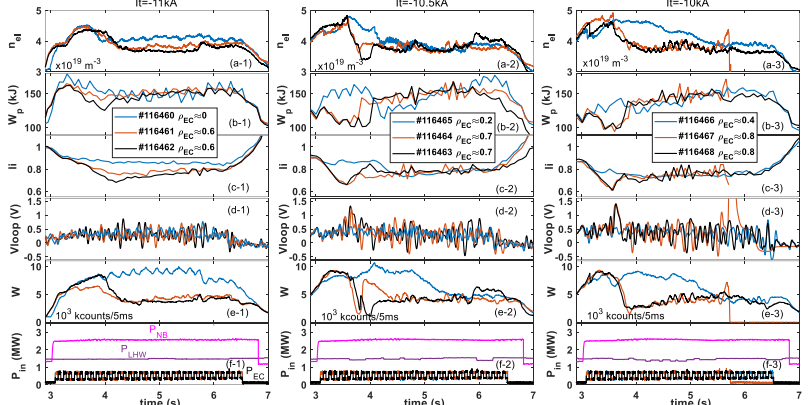


FIG. 1. Temporal evolutions of discharge parameters during the ECRH edge deposition experiments, illustrating (a-1, 2, 3) line average plasma density, (b-1, 2, 3) plasma stored energy, (c-1, 2, 3) the internal induction, (d-1, 2, 3) the loop voltage, Vloop, (e-1, 2, 3) the tungsten impurity measured by extreme ultraviolet (EUV)[13], and (f-1, 2, 3) injected auxiliary heating power, where the pink and purple lines are corresponding to the NBI and LHCD power, the modulated power is ECRH. The numbers 1, 2 and 3 correspond to the toroidal magnetic coil current $I_t = -11kA$, -10.5kA and -10kA, respectively. Since the ECRH power was modulated, the electron cyclotron emission (ECE)[14] diagnostic measured the resulting perturbed temperature δT_e profiles for the three I_t cases, as illustrated in Fig. 2. In this figure, δT_e is selected near the modulation frequency of 5 Hz, after performing Fourier decomposition on the fluctuations of the electron temperature. The extreme point of the δT_e profile indicates the ECRH deposition position, which gradually shifted to the outward as the toroidal magnetic field decreased. This observation is consistent with the configured ECRH mirror setting. In addition, there is evident that the amplitude of the temperature perturbations decrease significantly as the ECRH deposition position moves closer to the plasma edge.

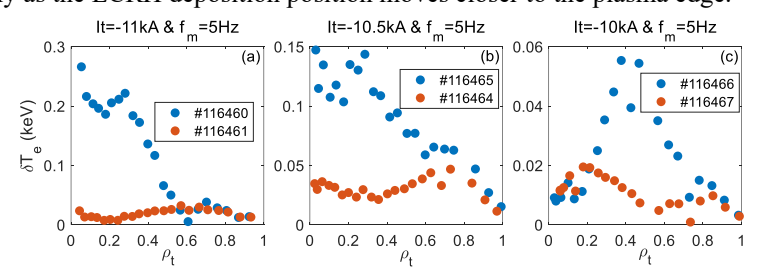


FIG. 2. Profiles of the perturbed electron temperature measured by ECE induced by 5 Hz ECRH power modulation, where panels (a), (b) and (c) correspond to the I_t platforms of -11kA, -10.5kA and -10kA, respectively.

Focusing on the operational point $I_t = 10kA$, where ECRH was deposited at $\rho_{EC} \approx 0.4$ and $\rho_{EC} \approx 0.8$, the detailed evolution of plasma parameters toward an improved confinement stage is presented in Fig. 3. After the off-axis ECRH deposition, both core (Fig. 3(a)) and edge (Fig. 3(b)) plasma density decreased. Concurrently, the plasma ion (Fig. 3(d)) and electron temperature (Fig. 3(g, h)) gradually increased. The relative toroidal velocity (Fig. 3(e)), as measured by X-ray crystal spectrometer (XCS)[15], initially increased and then returned to its pre-ECRH heating level. Core plasma turbulence (Fig. 3(i)), measured by the PCR[16] diagnostic, exhibited a gradual reduction until a constant state. Moreover, the core plasma density gradient (Fig. 3(j)), estimated by the core and

edge polarimeter/interferometer (POINT)[17] chords, gradually decreased until reaching a steady state. In the steady state case, this evolution resulted in improved plasma performance, characterized by increased plasma stored energy (Fig. 3(c)), lower level of tungsten impurities (Fig. 3(f)), and reduced turbulence fluctuations. Notably, for $\rho_{EC} \approx 0.8$ cases, the transition to steady state occurred much more rapidly than for $\rho_{EC} \approx 0.4$. And the plasma confinement was first transitioned to L-mode and then returned to H-mode, as evidenced by the abrupt decrease and subsequent recovery of edge plasma density (see Fig. 3(b)).

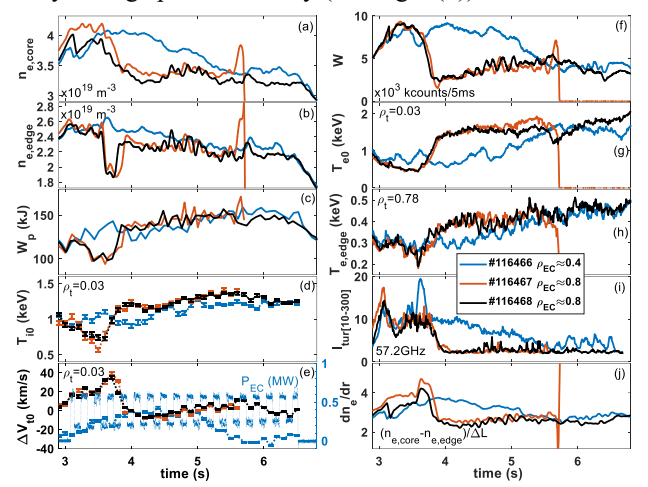


FIG. 3. Temporal evolutions of plasma parameters during the experiment: (a) core and (b) edge line-averaged plasma density, (c) plasma stored energy, (d) core ion temperature, (e) core relative toroidal rotation, (f) tungsten impurity level measured by the EUV diagnostic, (g) core and (h) edge electron temperature, (i) turbulence intensity at 57.2GHz measured by the PCR diagnostic, and (j) plasma electron density gradient estimated from POINT measurements.

The suppression of tungsten central accumulation is strongly related to the plasma density and ion temperature gradient, as well as toroidal rotation, as illustrated in Fig. 4. This figure shows a gradual decrease in tungsten impurity levels over time. Concurrently, the averaged normalized density gradient length $\langle \frac{R_0}{L_{ne}} \rangle$, estimated by POINT, gradually decreased, while the averaged normalized ion temperature gradient length $\langle \frac{R_0}{L_{Ti}} \rangle$, estimated by XCS, increased with time for all three cases. According to a simplified analytical model presented in ref. [18], the normalized impurity gradient length $\frac{R_0}{L_{n_Z}}$ is proportional to the ratio of impurity neoclassical convection $V_{Z,neo}$

to diffusion
$$D_{Z,neo}$$
, which can be approximated by $\langle \frac{R_0}{L_{ne}} \rangle$ and $\langle \frac{R_0}{L_{Ti}} \rangle$ as follows,
$$\frac{R_0}{L_{nz}} \propto \frac{R_0 V_{Z,neo}}{D_{Z,neo}} \approx -Z(\langle \frac{R_0}{L_{ne}} \rangle - 0.5 \langle \frac{R_0}{L_{Ti}} \rangle)$$
 (1) where R_0 the major radius at magnetic axis. The quantity of $\frac{R_0 V_{Z,neo}}{ZD_{Z,neo}}$ initially increased and subsequently decreased to a small value during the improved confinement phase. Meanwhile, the core relative toroidal rotation

decreased to a small value during the improved confinement phase. Meanwhile, the core relative toroidal rotation decreases over time, which is expected to weaken tungsten poloidal asymmetry, thereby further reducing central tungsten accumulation [19].

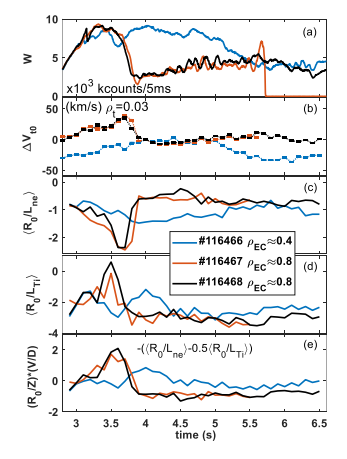


FIG. 4. Temporal evolutions of plasma parameters: (a) tungsten impurity, (b) relative toroidal velocity, (c) averaged normalized plasma density gradient length $\langle \frac{R_0}{L_{ne}} \rangle$, (d) averaged normalized plasma ion temperature gradient length $\langle \frac{R_0}{L_{Ti}} \rangle$, (e) neo-classical pitch parameter, $\frac{R_0 V_{Z,neo}}{D_{Z,neo}} \approx -Z(\langle \frac{R_0}{L_{ne}} \rangle - 0.5 \langle \frac{R_0}{L_{Ti}} \rangle)$.

2.2. Plasma profile evolution

During the improved confinement phase, both the electron temperature and its gradient were substantially enhanced. As shown in Fig. 5, following the edge ECRH power deposition, the electron temperature gradually increased, with the core temperature nearly doubling in the improved confinement stage. The electron temperature gradient and its normalized gradient length gradually increased over time, reaching saturation around 5.5 s. At this saturated stage, the maximum temperature gradient was observed near $\rho_t \sim 0.4$, corresponding closely to the ECRH power deposition location.

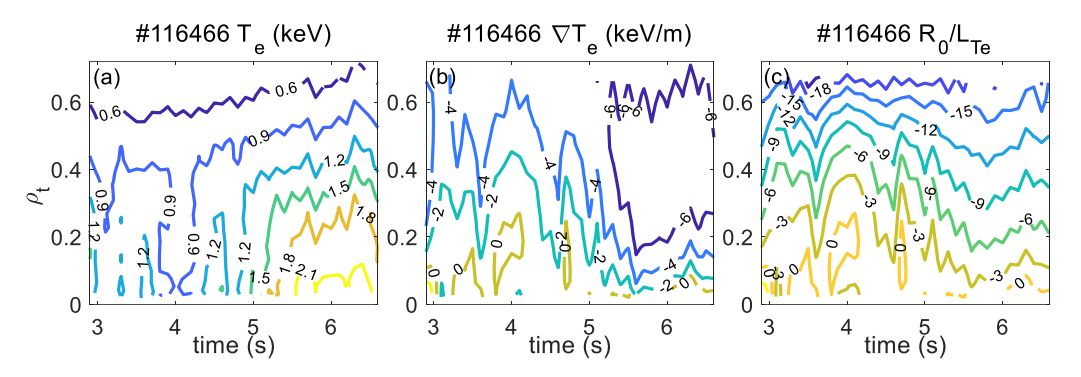


FIG. 5. Contour plots of (a) electron temperature, (b) electron temperature gradient, and (c) normalized electron temperature gradient length as functions of radial position and time. The electron temperature is measured by ECE.

Characteristic plasma profiles before and after the transition to the improved confinement state are presented in Fig. 6, with time slices at 4.05s and 6.05s for discharge #116466. Following the evolution to the improved confinement regime, the core plasma is significantly reduced, accompanied by notable increases in both ion and electron temperatures. The electron temperature in the core nearly doubles, and the ion temperature rises substantially. Moreover, the plasma toroidal velocity decreases considerably, particularly in the central region. Note that these measurements were obtained using complementary diagnostic techniques: density profiles were estimated via POINT analysis, electron temperature was measured by Thomson Scattering (TS)[20], and both ion temperature and toroidal velocity were determined by Charge Exchange Recombination Spectroscopy (CXRS)[21].

The safety factor profile, estimated by POINT diagnostic via measuring the Faraday rotation angle, is presented in Fig. 7. Following ECRH injection, the safety factor exhibited an initial increase in the core region until establishing a negative magnetic shear configuration at ~4 s, where the minimal safety value was localized at ρ_t ~0.4. After sustaining ~0.5s, the core safety factor gradually decreased, and returned to its original state. This temporal evolution provides insight into the dynamic reconfiguration of the plasma's magnetic structure during the off-axis ECRH experiment.

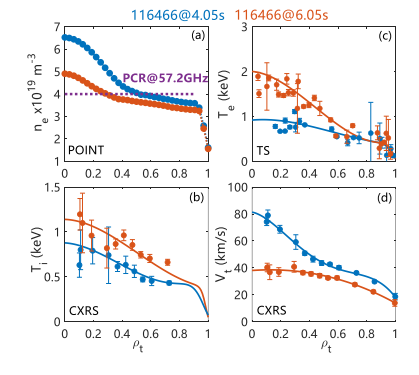


FIG. 6. Plasma profiles of (a) plasma density and PCR measurement position for frequency 57.2GHz, (b) ion temperature, (c) electron temperature, and (d) toroidal velocity. Note that the blue and red colors correspond to time slices at 4.05s and 6.05s, respectively, for discharge #116466, where ECRH was deposited at $\rho_t = 0.4$.

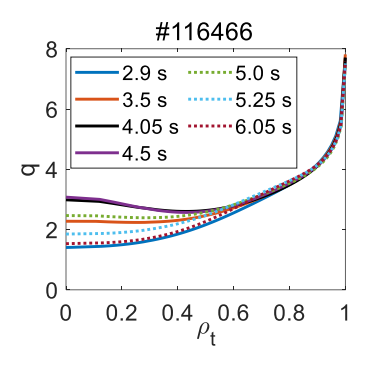


FIG. 7. Profiles of the safety factor estimated at various times in discharge #116466.

2.3. Measurement of turbulence evolution

The PCR diagnostic detected an electrostatic turbulence propagating in the ion diamagnetic direction at the measurement location of $\rho_t \approx 0.3-0.5$, as shown in Fig. 8. Following the ECRH injection, the intensity of the low-frequency broadband turbulence gradually decreased from ~3.8s to ~5.5s. During this period, both the core electron (red line) and ion temperature (red dot) exhibited a gradual increase, while the core plasma density and tungsten impurity gradually decreased. Cross-power spectral analysis during the interval t = 3.5-4.5s revealed that the turbulence frequency spectrum peaked near zero frequency and propagated in the ion diamagnetic direction. These characteristics suggest that the observed turbulence is attributed to ITG instability. And the reduction in its intensity starting at ~3.8s is probably caused by the onset of negative magnetic shear at the core. Note that the measurement position of the PCR diagnostic is dependent on the plasma density, which shifted from $\rho_t \sim 0.5$ to $\rho_t \sim 0.3$ as the plasma density gradually decreased from ~4.2s to ~5.5s during the experiment.

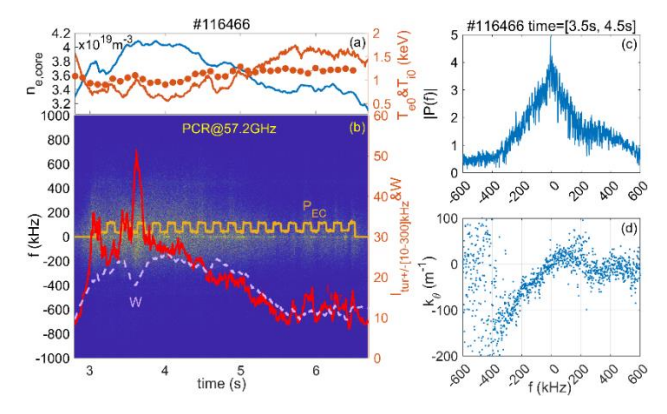


FIG. 8. Temporal evolutions of (a) line-averaged plasma density (blue line), core ion (red dot) and electron temperature (red line); (b) turbulence power spectrum and its intensity (red line) at core plasma for channel 57.2GHz, ECRH power (yellow line) and tungsten impurity (purple dashed line); Ensemble-averaged spectra over the interval t = [3.5, 4.5] s of (c) turbulence power and (d) wavenumber.

3. THEORETICAL SIMULATION

We have conducted a theoretical simulation by means of TGLF and NEO to study the turbulence characteristic and the tungsten transport. The results are present in the following sections.

3.1. Turbulence characteristic

To identify the turbulence characteristic, we performed the TGLF-SAT1 simulation [22], with results presented in Fig. 9. This figure displays the linear growth rate multiplied by the sign of the turbulence frequency as functions of wavenumber $k_{\theta}\rho_{s}$ and radial position for discharge #116466 at time 4.05s and 6.05s. The positive value,

colored in red, corresponds to modes propagating in the electron diamagnetic drift direction, while negative value indicates propagation in the ion diamagnetic drift direction. As seen in Fig. 9(a), which corresponds to time 4.05s, there is TEM in the core region ($\rho_t < 0.45$) and ITG at the edge region (0.45 < $\rho_t < 0.7$). After the plasma evolved to the improved confinement stage, as shown in Fig. 9(b), the core TEM region is shrunk, and its growth rate is also decreased. Simultaneously, the edge ITG region is expanded. Note that there is also co-existed ETG turbulence in the high $k_{\theta}\rho_s$ region which is also colored in red. The expansion of the ITG region is consistent with the PCR measurement as shown in Fig. 8, where the PCR diagnostic has measured an electrostatic turbulence propagating along ion diamagnetic drift direction, with its position initially at $\rho_t \approx 0.5$ and then shifted to $\rho_t \approx 0.3$ due to the decrease of plasma density.

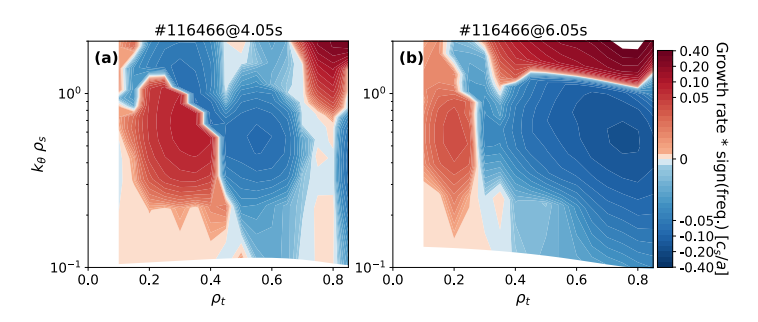


FIG. 9. Linear growth rate times the sign of frequency of turbulence as functions of wavenumber $k_{\theta}\rho_{s}$ and radius for discharge #116466 at time (a) 4.05s and (b) 6.05s.

To assess the sensitivity of the turbulence linear growth rate, we performed a parameter scan by varying the normalized gradient lengths of plasma density, ion and electron temperature, as well as the ion-to-electron temperature ratio by $\pm 20\%$ from their baseline values. The results, shown in Fig. 10, reveal that the TEM turbulence at $\rho_t = 0.3$ becomes more unstable with increasing a/L_{ni} , while it is stabilized as a/L_{Ti} and T_i/T_e increase. In contrast, the ITG turbulence at $\rho_t = 0.5$ becomes more unstable as a/L_{Ti} increases, but is stabilized as T_i/T_e increased. These results indicate that the TEM turbulence in #116466 is primarily driven by the plasma density gradient, whereas the ITG turbulence is driven by the ion temperature gradient. The density gradient driven trapped electron mode (DGTEM) turbulence has ever been observed in Alcator C-mod [23] and DIII-D [24], where it was shown to be destabilized by the density gradient and T_e/T_i ratio, and suppressed by negative magnetic shear.

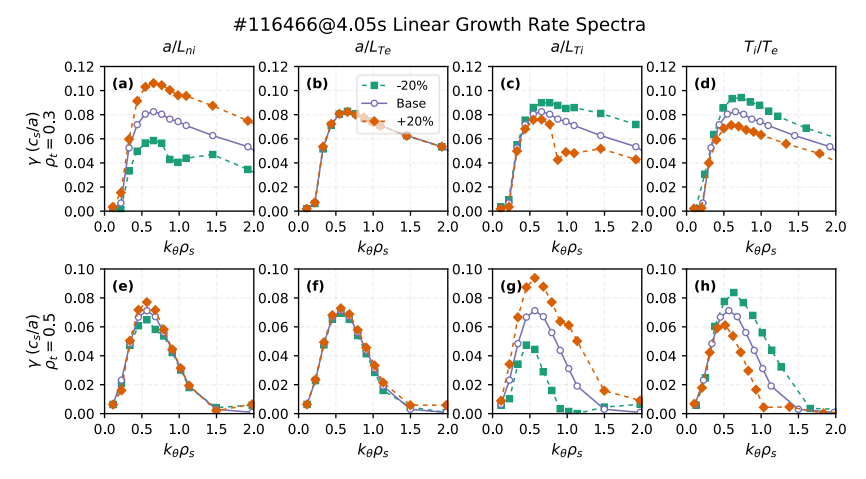


FIG. 10. The linear growth rate spectra as a function of $k_{\theta}\rho_s$ for various plasma parameters: (a) and (e) normalized density gradient α/L_{ni} , (b) and (f) normalized electron temperature gradient α/L_{Te} , (c) and (g) normalized ion temperature gradient α/L_{Ti} , (d) and (h) T_i/T_e . Note that the subfigures (a)-(d) are at $\rho_t = 0.3$, and the subfigures (e)-(h) are at $\rho_t = 0.5$. Blue circles represent results computed using the baseline experimental parameters, whereas green squares and orange diamonds denote results decreased and increased by 20% from the baseline, respectively.

Figure 11 presents the maximum growth rate of the TEM turbulence at $\rho_t = 0.3$ as functions of the plasma density gradient and magnetic shear, and the maximum growth rate of the ITG turbulence at $\rho_t = 0.5$ as functions of the ion temperature gradient and magnetic shear. The red dashed line denotes the experimental value. As shown, both TEM and ITG exhibit a critical gradient threshold of approximately unity for the normalized

density and ion temperature gradient lengths, respectively. When the experimental values exceed this threshold, the growth rates of both TEM and ITG increase significantly. Moreover, adjusting the magnetic shear from positive to negative reduces the turbulence growth rate, particularly for ITG turbulence, as illustrated in Fig. 11(d). This is consistent with the theory that negative magnetic shear can suppress both TEM [25] and ITG [26] turbulences. This result suggests that the improvement in plasma performance is correlated with the formation of negative magnetic shear, which effectively mitigates TEM and ITG turbulence.

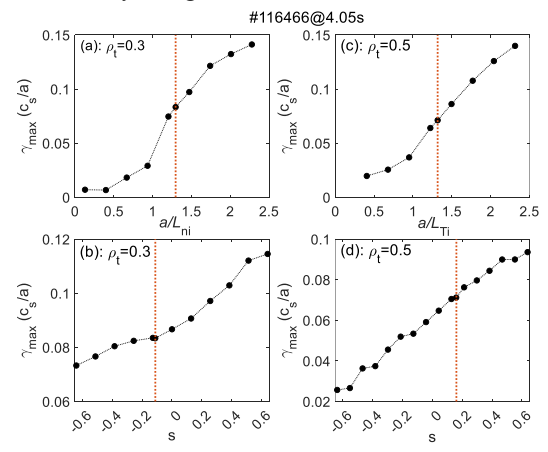


FIG. 11. The maximum linear growth rate γ_{max} as a function of (a) α/L_{ni} and (b) magnetic shear s at $\rho_t = 0.3$, and (c) α/L_{Ti} and (d) s at $\rho_t = 0.5$.

3.2. Tungsten neo-classical transport

Reducing TEM and ITG turbulence can reduce the electron and ion heat transport, which in turn allows for an increase in the electron and ion temperature gradients. Consequently, this results in an increase in the core electron and ion temperature. All of these are helpful to improve the plasma confinement and reduce the tungsten inward convective velocity. To quantitatively study the tungsten transport, a NEO simulation was performed and shown in Fig. 12. The NEO analysis shows that both tungsten diffusion and convective velocity are significantly diminished. In combination, the overall drift parameter v/D, which is proportional to the tungsten density gradient, is substantially lowered at time 6.05s, as shown in the lower panel. As a result, the W central accumulation has been suppressed.

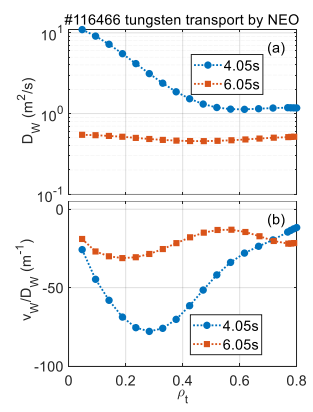


FIG. 12. Profiles of tungsten impurity 27+ diffusion coefficient (a) and drift parameter (b) for the modelling of discharge #116466.

4. CONCLUSION

In summary, the edge ECRH power deposition experiment has been observed to improve plasma performance in the EAST tokamak. During LHCD and NBI heating in H-mode plasma, 0.6 MW of ECRH power, modulated at 5 Hz and 10 Hz, was deposited from the core ($\rho_{EC} \sim 0$) to the edge ($\rho_{EC} \sim 0.8$) by adjusting the ECRH mirror and reducing the toroidal magnetic field. Perturbed temperature profiles measured by the ECE diagnostic exhibited maxima that closely correlated with the ECRH deposition locations. Following the edge ECRH deposition, both plasma density and tungsten impurity levels gradually decreased, whereas plasma electron and ion temperatures, as well as stored plasma energy, gradually increased. This resulted in a flattened plasma density profile and steeper

IAEA-CN-316/INDICO ID #2895

electron and ion temperature gradients. These changes contributed to a reduction in the neo-classical pitch velocity of tungsten. Concurrently, the core safety factor, as estimated by POINT, was observed to gradually increase, inducing a negative magnetic shear that persisted for approximately one second, before recovering to positive magnetic shear in the improved confinement stage. The turbulence intensity, whose location shifted from $\rho_t \approx 0.5$ to $\rho_t \approx 0.3$ as plasma density gradually decreased, was observed to gradually decrease during the negative magnetic shear stage, which was began at ~3.8s. Here, the turbulence, which was identified as electrostatic, propagated in the ion diamagnetic direction, suggesting the presence of ITG instability.

Theoretical simulations using TGLF, and NEO generally supported these findings. The TGLF-SAT1 result reveals that there are a density gradient driven TEM turbulence in the core ($\rho_t < 0.45$) and an ITG turbulence at the edge ($\rho_t > 0.45$). As the plasma confinement improved, the TEM region is shrunk, with a decrease of linear growth rate, while edge ITG region is expanded. Adjusting the magnetic shear from the positive to negative can reduce the TEM and ITG turbulence growth rate. NEO results show that tungsten convective velocity is significantly reduced, leading to a significant reduction in tungsten neoclassical transport. These results may help to extend the operational range of ECRH in future high-field fusion devices without deteriorating the plasma confinement.

ACKNOWLEDGEMENTS

The authors deeply appreciate the continued research and operational efforts of the entire EAST teams. Author Y. L. Li appreciates X. Q. Wu, Y. C. Li, Z. Y. Si, C. J. Xiao, Tomáš Odstrčil, C. B. Wu, Y. X. Cheng, L. Ye, Y. H. Huang, J. L. Chen, S. T. Mao, M. H. Li, and X. Jian for valuable discussions. This work has been supported by the National Magnetic Confinement Fusion Energy R&D Program of China under Grant No. 2022YFE03020004, 2019YFE03030000. We thank the staff members at EAST in Hefei (https://cstr.cn/31130.02.EAST), for providing technical support and assistance in data collection and analysis.

REFERENCES

- [1] Schmid K. and Wauters T. 2024 Nucl. Mater. Energy 41 101789
- [2] Neu R. et al. 2002 Plasma Phys. Control. Fusion 44 811
- [3] Angioni C. et al. 2017 Nucl. Fusion **57** 056015
- [4] Sertoli M. et al. 2017 Phys. Plasma 24 112503
- [5] Shi S. et al. 2022 Nucl. Fusion 62 066031
- [6] Peeters A. G. et al. 2005 Phys. Plasma 12 022505
- [7] Burckhart A. et al. 2016 Nucl. Fusion 56 056011
- [8] Rossel J. X. et al. 2012 Nucl. Fusion **52** 032004
- [9] Smith S. P. et al. 2015 Nucl. Fusion **55** 083011
- [10] Gong X. et al. 2024 Nucl. Fusion **64** 112013
- [11] Staebler G. M. et al. 2007 Phys. Plasma 14 055909
- [12] Belli E. A. and Candy J. 2008 Plasma Phys. Control. Fusion 50 095010
- [13] Zhang L. et al. 2015 Rev. Sci. Instrum. 86 123509
- [14] Liu Y. et al. 2018 Fusion Eng. Des. 136 72-75
- [15] Lyu B. et al. 2014 Rev. Sci. Instrum. 85 11E406
- [16] Qu H. et al. 2016 Rev. Sci. Instrum. 87 11E707
- [17] Liu H. Q. et al. 2016 Rev. Sci. Instrum. 87 11D903
- [18] Angioni C. et al. 2015 Phys. Plasma 22 055902
- [19] Angioni C. and Helander P. 2014 Plasma Phys. Control. Fusion 56 124001
- [20] Zang Q. et al. 2013 Rev. Sci. Instrum. 84 093504
- [21] Ye M. et al. 2015 Fusion Eng. Des. 96-97 1017
- [22] Staebler G. M. et al. 2016 Phys. Plasma 23 062518
- [23] Ernst D. R. et al. 2004 Phys. Plasma 11 2637
- [24] Ernst D. R. et al. 2016 Phys. Plasma 23 056112
- [25] Li J. Q. and Kishimoto Y. 2002 Plasma Phys. Control. Fusion 44 A479
- [26] Antonsen T. M. et al. 1996 Phys. Plasma 3 2221